

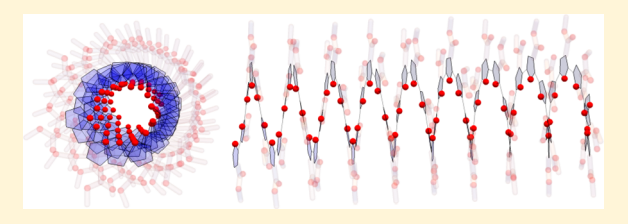
Photostable Helical Polyfurans

Anthony J. Varni, Andria Fortney, Matthew A. Baker, Joshua C. Worch, Yunyan Qiu,[®] David Yaron,[®] Stefan Bernhard, Kevin J. T. Noonan, and Tomasz Kowalewski to

Department of Chemistry, Carnegie Mellon University, 4400 Fifth Avenue, Pittsburgh, Pennsylvania 15213-2617, United States

Supporting Information

ABSTRACT: This report describes the design and synthesis of a new class of polyfurans bearing ester side chains. The macromolecules can be synthesized using catalyst-transfer polycondensation, providing precise control over molecular weight and molecular weight distribution. Such obtained furan ester polymers are significantly more photostable than their alkyl analogues owing to the electron-withdrawing nature of the attached subunit. Most interestingly, they spontaneously fold into a compact π -stacked



helix, yielding a complex multilayer cylindrical nanoparticle with a hollow, rigid, conjugated core composed of the polyfuran backbone and a soft, insulating outer layer formed by the ester side chains. The length of polymer side chains dictates the outer diameter of such nanoparticles, which for the hexyl ester groups used in the present study is equal to ~2.3 nm. The inner cavity of the conjugated core is lined with oxygen atoms, which set its effective diameter to 0.4 nm. Furthermore, installation of bulkier, branched chiral ester side chains on the repeat unit yields structures that, upon change of solvent, can reversibly transition between an ordered chiral helical folded and disordered unfolded state.

■ INTRODUCTION

The current study was aimed at designing a synthetic strategy that would circumvent a long-standing limitation in the use of furan repeat units in conjugated systems, stemming from its inferior photostability.^{1,2} This goal was accomplished by the attachment of electron-withdrawing ester groups to furan monomers, which are subsequently polymerized using living catalyst-transfer polycondensation (CTP).³⁻⁹ Notably, this substitution resulted in robust foldamers, 10-14 where the polymer chains adopted tightly packed helical structures. 15

In order to comprehensively address these aspects, the results are presented in the following order. First, the decomposition of a hexyl-substituted polyfuran is discussed, to illustrate the stability challenges of this conjugated building block. Subsequently, the synthetic methods to obtain the estersubstituted polyfuran are described and the experimental observations that indicate the polymerization was living. The photostability of the furan ester polymer was probed using two separate experiments to establish its tolerance toward singlet $O_2(^1\Delta_g)$. The description of the synthesis and stability is then followed by the extensive discussion of computational work as well as physical characterization of the polymer.

Factors Underlying Limited Photostability of Conjugated Furans. Over the past few decades, linear macromolecules based on five-membered heteroaromatic rings emerged as one of the canonical families of conjugated polymers, dominated by thiophene repeat units.¹⁶ Furan is notably underrepresented within this family due to the insufficient photostability of its conjugated species. The ongoing desire to utilize furan as a building block for conjugated architectures is driven by its solubility, strong luminescence, and the possibility to source it from biorenewables. 17-23 Moreover, the small size of the ring oxygen alleviates steric strain in extended π -systems composed of rings substituted with side groups for solubility. 24,25 This can enhance planarization and electronic properties. 26,27

Given all these considerations, furan remains an extremely attractive target in organic materials. To understand the origin of furan's limited photostability, it is useful to compare the structure of furan and thiophene. Geometrically, the furan ring is smaller than its thiophene counterpart with shorter C-X bonds, making the entire 6π -electron system more confined. Likewise, the HOMO energy of furan is higher than thiophene $(-6.50 \text{ eV versus } -8.93 \text{ eV from DFT at } 6-31\text{G}^{++})$. The combination of these factors makes the furan C=C bonds significantly more susceptible to reactions with singlet O_2 . $^{28-30}$ The endoperoxide product of this reaction for furan is known to readily undergo bond breaking, yielding other organic derivatives. 28-30 While this type II photooxidation is widely utilized in organic synthesis to form new molecules, it is highly detrimental for stability of furan-containing conjugated chains.

RESULTS AND DISCUSSION

Photodegradation of P3HF. The rapid photodegradation of poly(3-hexylfuran) (P3HF) in solution is evident from a color change when the solution is exposed to visible light. It was quantified by the time evolution of UV-vis absorption spectra shown in Figure 1. The observed disappearance of the absorption maximum at 460 nm and appearance of a broad feature at 375 nm is indicative of a loss of conjugation.

Received: February 10, 2019 Published: April 30, 2019



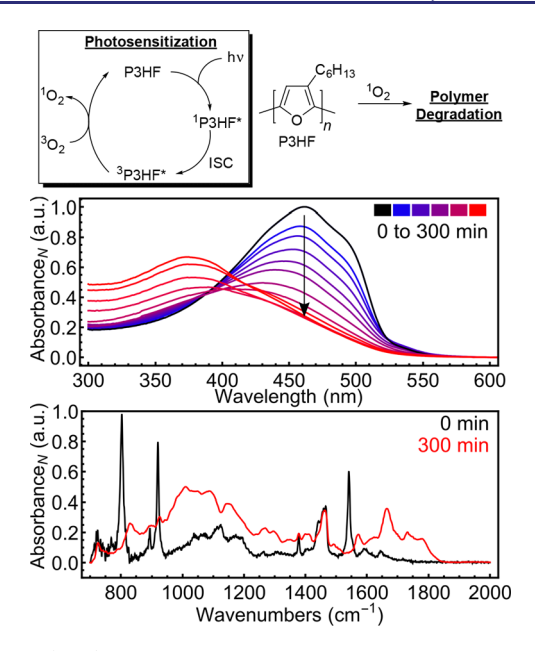


Figure 1. (Top) Photosensitization scheme of P3HF decomposition with visible light. (Middle) Normalized UV—vis absorption spectra of P3HF and its relative change in peak intensity over time after visible light irradiation in air. Black trace corresponds to time = 0 min and red trace is after 300 min. (Bottom) Normalized absorbance of FTIR spectrum (2000–700 cm⁻¹) before and after visible light irradiation.

Accordingly, comparison of FTIR spectra of the polymer before and after 5 h exposure to visible light reveals the disappearance of a $\nu_{C=C}$ stretch corresponding to the furan ring (1542 cm⁻¹) and an appearance of three stretches tentatively assigned as $\nu_{C=0}$ bands at 1667, 1734, and 1781 cm⁻¹. Such structural changes are consistent with P3HF acting as a photosensitizer, generating ¹O₂, and degrading via addition with this reactive species. This attribution of polymer degradation to ¹O₂ was confirmed by control experiments under N2 which did not reveal similar changes in thoroughly deoxygenated P3HF solutions (Figure S51). ¹H NMR and IR of the degraded sample were inconclusive as to the exact degradation pathways and products (Figure S50), perhaps because each furan ring within the polymer backbone is a potentially reactive site for ¹O₂. Further investigations are ongoing.

Ester-Substituted Polyfuran. To combat the instability of P3HF, the electron-donating alkyl group was replaced with an electron-withdrawing ester group. We had developed a synthetic method to access poly(3-hexylesterthiophene) previously,³¹ and we envisioned an analogous protocol to obtain the related furan polymer (poly(3-hexylesterfuran) or P3HEF). A Suzuki-Miyaura-type monomer (1, Table 1) was synthesized in a three-step reaction sequence with a bromine and pinacol boronate at the 2 and 5 positions of the furan ring, respectively. A detailed description of the monomer synthesis can be found in the Supporting Information, and the procedure was nearly identical to the synthesis of the previous thiophene derivative. 31 We conducted polymerizations in the presence of a commercially available N-heterocyclic carbene (NHC) nickel complex, as we had noted in our prior work that this catalyst was able to drive controlled polymerization of the ester thiophene monomer. ³¹ The high σ -donor strength of the NHC has been hypothesized to facilitate catalyst transfer to the polymer chain-end after each monomer addition. 32,33 Polymer-

Table 1. Preparation of Ester-Substituted Polyfuran

$$C_6H_{13}O$$
 $C_1-N_1-C_1$
 $C_6H_{13}O$
 $C_1-N_1-C_1$
 $C_6H_{13}O$
 $C_1-N_1-C_1$
 $C_6H_{13}O$
 $C_1-N_1-C_1$
 C_1-

entry	cat. (mol %)	time (min)	$M_{\rm n}$ (kDa)	Đ	yield (%)
1	4	30	4.1	1.07	89
2	2.5	45	5.8	1.07	73
3	1	60	10.2	1.12	88

^aGPC traces were recorded versus polystyrene standards at 40 °C with THF as the eluent.

ization of monomer 1 was carried out in tetrahydrofuran (THF) with 2 equiv of cesium fluoride as the base and a small portion of water (0.2 mL) at 50 °C (Table 1). We had previously employed K₃PO₄·H₂O as the base,³¹ but in this case, we obtained higher molecular weights and better yields using CsF. Polymerizations proceeded quickly (1 h or less), and termination of the reaction was carried out by precipitation and quenching using 6 M HCl in MeOH. The final polymers were washed with MeOH and H2O prior to analysis by gel permeation chromatography (GPC). The obtained narrow molar mass distributions and the observed dependence of M_n on monomer to catalyst ratio (entries 1–3) provide strong evidence that the polymerization proceeded in a chain-growth fashion. However, loadings of below 1% for the Ni-NHC precatalyst did not increase $M_{\rm p}$, suggesting 1% is the limit for effective polymerization. Further confirmation of chain growth was provided by the linear increase of M_n with conversion with preservation of narrow dispersity (Figure 2, left). $^{3-9}$

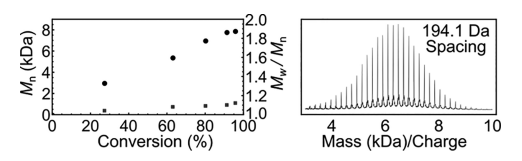


Figure 2. Left: M_n (black circles) versus conversion for a polymerization conducted with 2 mol % catalyst (0.03 M = [1]). Dispersity values are shown as blue squares. Right: MALDI-TOF mass spectrum of P3HEF sample from Table 1, entry 1.

MALDI-TOF mass spectrometry confirmed that only one set of polymer end groups was present (terminal H and Br groups) as expected for this type of polymerization mechanism (Figure 2, right). Notably, the $M_{\rm n}$ value obtained from GPC for P3HEF was lower than that obtained by MALDI-TOF (4.1 vs 6.2 kDa). This is in stark contrast to what is observed for polymers such as poly(3-hexylthiophene), where GPC analysis tends to overestimate molecular weight. The highly compact structure implied by the low value of $M_{\rm n}$ obtained by GPC was the first indication of the unusual conformational properties of P3HEF.

Further indication of this unusual conformational behavior was also evident from the massive line broadening in the ¹H and ¹³C NMR spectra of P3HEF (e.g., 700 Hz for the aromatic proton versus 40 Hz observed for the polythiophene analogue shown in Figure 3). ³¹ As discussed in the second half of this article, the likely origin of this broadening is the

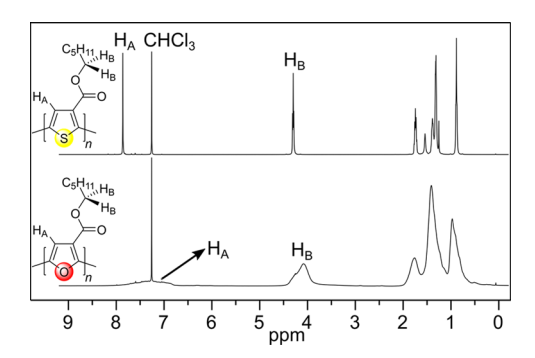


Figure 3. 1 H NMR spectra (500 MHz) of P3HET (32.9 kDa) and P3HEF (6.9 kDa) acquired at 22 $^{\circ}$ C in CDCl₃.

restricted tumbling motion of the polymer in solution caused by its compact folded conformation. Notably, the observed broadening could not be diminished by carrying out the NMR experiments at temperatures as high as 80 °C. The ¹³C NMR, while also broad, produced distinct resonances confirming the microstructural assignment of the polymer. The carbon atoms adjacent to the ring oxygen appeared at 146.1 and 141.0 ppm (Figure S25), and the carbonyl signal was observed at 161.3 ppm.

Improved Photostability of P3HEF. Photostability of P3HEF was assessed in an identical manner to P3HF. In contrast to P3HF, UV—vis and FTIR (Figure S53) spectra of P3HEF remained virtually unchanged over the course of irradiation (5 h). Two possible explanations of such an improvement could be inefficient singlet oxygen generation by P3HEF (e.g., due to less efficient intersystem crossing) or suppression of reactivity with singlet O₂. The latter explanation is favored by the absence of marked changes in the UV—vis spectra of P3HEF acquired in the presence of Rose Bengal (RB), a potent singlet oxygen generator (Figure 4). It should

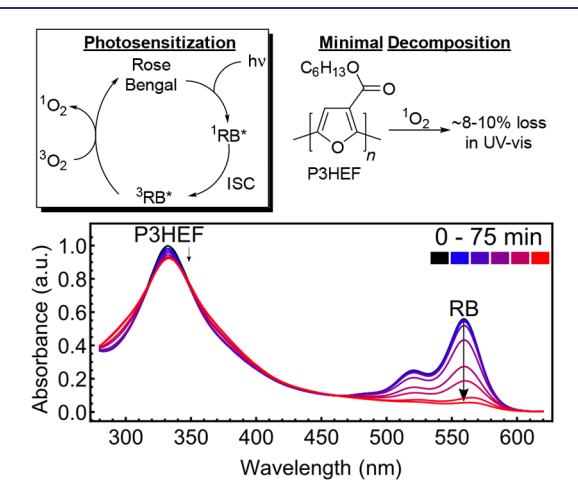


Figure 4. UV—vis photodegradation absorbance profiles of P3HEF (331 nm) in the presence of Rose Bengal (560 nm).

be noted that the distinct feature above 450 nm corresponds to the spectrum of RB. The resistance of P3HEF to singlet oxygen is highlighted by the near complete loss of the RB feature from the spectrum upon prolonged irradiation, pointing to its degradation by singlet oxygen. No observations of an O₂ intermediate have been obtained to date with P3HEF, but reversible addition of 1 O₂ to these polymer structures cannot be ruled out. Future work on these materials will be

focused on a more detailed photochemistry picture using discrete model systems.

DFT Investigation. The spectroscopic characterization of P3HEF (Figures 3 and 4) raises some important questions regarding the nature of this polymer. To begin with, the NMR spectra are very broad, nearly preventing accurate structural determination. Furthermore, the UV-vis spectrum tails in the visible region and the absorption maximum does not show the red-shift expected for extended conjugation. These features suggest a disordered or degraded sample. However, this is in contradiction to the X-ray diffraction study shown below that suggests a highly ordered material. Our resolution to this apparent contradiction is that the polymer adopts a wellordered helical structure. The remainder of this article provides a detailed description of how this helical structure can account for all currently available characterization data. We begin with torsional potentials computed from density functional theory (DFT), which predict P3HEF to favor helices, while alkylsubstituted polyfuran favors linear geometries. In addition, computations of the UV-vis spectra agree well with experiment and provide an assignment of the transitions responsible for the observed low-energy tail.

Relaxed torsional potential energy scans of unsubstituted and 3,4'-substituted 2,2'-bifuran and bithiophene were from 0 to 180° with steps of 15° using DFT at the B3LYP-D3 6-31G(d,p) level (Figure 5). To aid comparison, the plots were shifted vertically to the energy maxima, which in all instances corresponded to a dihedral angle of 90°, where conjugation is completely broken. For unsubstituted 2,2'-bifuran, two local energy minima corresponded to coplanar arrangements of rings (anti or syn), with the global minimum occurring for the anti arrangement (red trace at the top of Figure 5). In contrast,

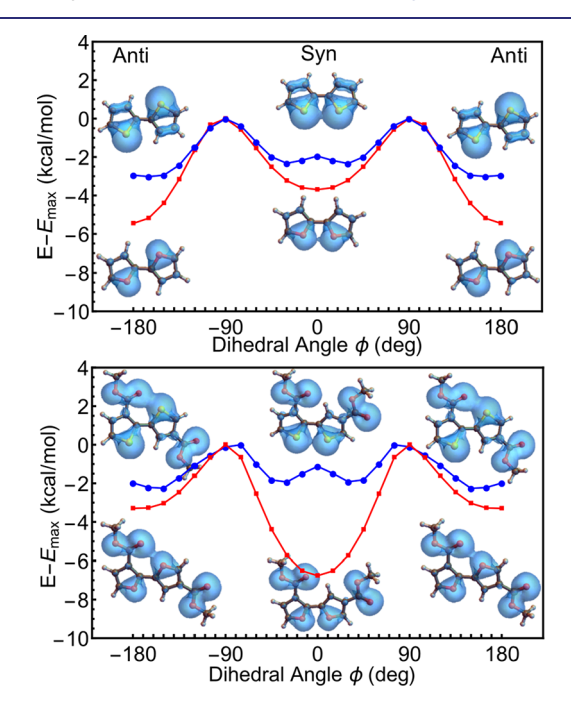


Figure 5. Torsional potential scans of dimers calculated by DFT at the B3LYP-D3 6-31G(d,p) level. (Top) 2,2'-Bifuran (red squares) and 2,2'-bithiophene (blue circles). (Bottom) 3,4'-Dimethyl ester-2,2'-bifuran (red squares) and 3,4'-dimethyl ester-2,2'-bithiophene (blue circles). The orbitals shown correspond to the lone pair electrons of heteroatoms and side groups to illustrate the origin of the steric constraints present when the rings are coplanar.

Journal of the American Chemical Society

Figure 6. Two views of the solid-state molecular structure of 3,4'-dimethyl ester-2,2'-bifuran. Thermal ellipsoids are at 50% probability. Complete crystallographic details are available in the Supporting Information.

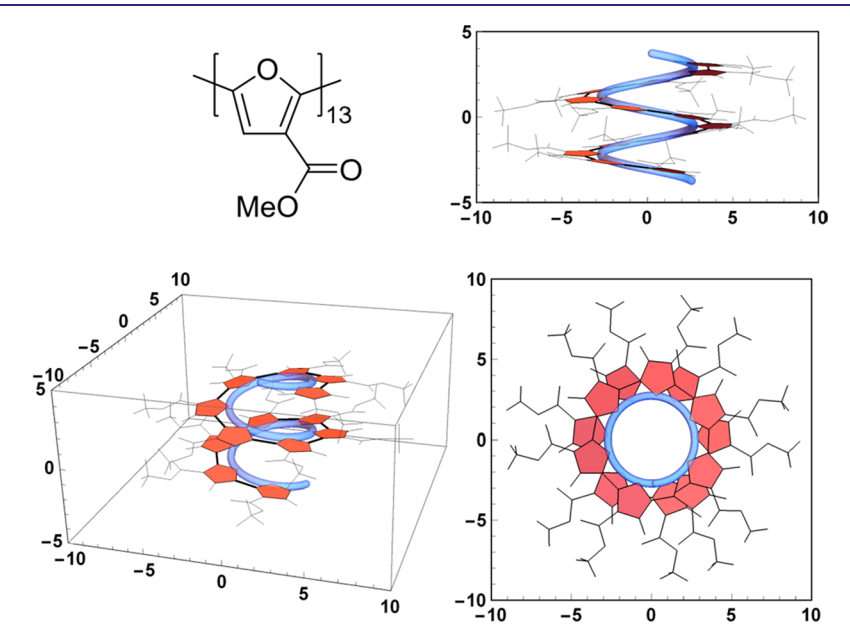


Figure 7. Helical structure of a tridecamer of furan methyl ester predicted by DFT at the B3LYP-D3 6-31G(d,p) level. Bounding boxes are scaled in angstroms (Å) and side chain contours are subdued for clarity. The pitch of the molecule was calculated to be ~ 3.4 Å, with 6.4 furan repeat units per turn. The computed energy difference between the HOMO and LUMO is equal to 2.5 eV.

for 2,2'-bithiophene, the lowest energy conformers were slightly twisted from the coplanar *anti* and *syn* forms, as reported previously.^{36–38} Importantly, the torsional potential barriers of bifuran markedly exceeded those for bithiophene.^{24,25,36} Similar relationships were observed for methylsubstituted dimers (Figure S40).

Remarkably, the torsional potential for bifuran changed dramatically upon the introduction of methyl ester side groups, with the *syn* conformation emerging as the global minimum with an energy nearly 3.5 kcal/mol lower than the *anti* conformer (red trace at the bottom of Figure 5). Such a strong *syn* preference is not present for bithiophene, where steric interactions between heteroatom lone pairs are almost equally unfavorable for both *anti* and *syn* conformations, giving preference to twisted nonplanar forms (blue trace at the bottom of Figure 5).

The *syn* preference for the 3,4'-dimethylester-2,2'-bifuran can be explained by the differences between molecular geometries of both conformers. In the *anti* conformation, the carbonyl and furan oxygens are 2.78 Å apart, which is less than the sum of their van der Waals radii (3.04 Å). The resulting repulsive interaction between the electron clouds of the oxygen lone pairs raises the relative potential energy of this conformation by about 2.2 kcal/mol in comparison with its unsubstituted counterpart, to -3.3 kcal/mol (both red traces in Figure 5). While this steric stress is relieved by rotating the

two rings out of plane, the twisting disrupts conjugation. The fully π -conjugated structure is recovered when the rings become coplanar again in the syn conformation, producing a local energy minimum. The ultimate energetic preference for the syn conformation in the methyl ester substituted dimer can be explained by the presence of the donor—acceptor interaction between the carbonyl oxygen lone pair and the hydrogen atom of the neighboring ring (3' position). The computed distance between these two atoms is only 2.2 Å, within the range of H-bonding.

To confirm this conformational preference experimentally, we synthesized and crystallized the 3,4'-dimethyl ester-2,2'-bifuran. As anticipated, the furan rings were in a syn conformation in the crystallized dimer with a slip-stacked arrangement in the unit cell (Figure 6). While crystal packing effects could impact the orientation of the rings, both computation and crystallography indicate that these substituted structures favor a syn configuration. The O-C-C-O angle between the two rings is equal to 4.9° , which is slightly larger than the dihedral angle from the computed optimized geometry (0°). The distance and angle between the carbonyl oxygen and nearby ring C-H bond (H···O=C) are respectively equal to 2.28 Å and 123.5° , implying an intramolecular H-bonding interaction.

If such strong preference of adjacent ester-substituted furan rings was to persist in longer oligomers, it would force them to Journal of the American Chemical Society

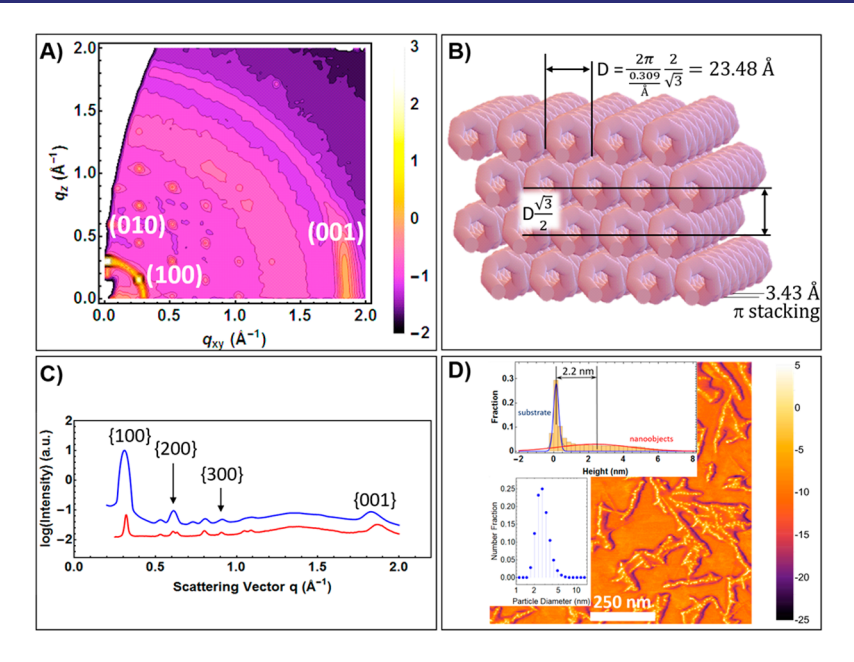


Figure 8. (A) Grazing incidence wide-angle X-ray scattering pattern obtained with the ultrathin film of P3HEF on silicon. (B) Schematic representation of hexagonal packing of helices giving rise to (010) and (100) reflections. The (001) reflection corresponds to the intrahelix π -stacking of polymer chains (3.43 Å). (C) Overlay of an azimuthally averaged GIWAXS pattern (blue trace) and of a powder diffraction pattern obtained with a precipitated polymer powder (red trace) demonstrating the prevalence of this packing format. (D) Phase contrast AFM image of P3HEF illustrating filamentous aggregates with a histogram of heights for the objects shown as a top inset and particle size distribution from DLS as a bottom inset. Scale bars for width and height are provided on the bottom and right, respectively.

adopt planar semicircular shapes (Figure S49). Furthermore, oligomers longer than 6 repeat units would have to form helical structures, ^{10–14,41–43} such as the one predicted by DFT for a tridecamer shown in Figure 7. This helical polyfuran consists of 6.4 repeat units per turn, has a pitch of 3.4 Å, and has a computed energy difference between the HOMO and LUMO levels of 2.5 eV. The helical structure of P3HEF was confirmed by powder diffraction patterns acquired using grazing incidence wide angle X-ray scattering (GIWAXS) of ultrathin films and by conventional X-ray powder diffraction (XRD) of precipitated polymers.

Solid-State Characterization. GIWAXS studies of P3HEF ultrathin films cast onto silicon wafers revealed hexagonal packing patterns attributed to π -stacked helical assemblies (Figure 8A). The center-to-center distance between helices (which corresponds to the helix outer diameter) calculated from the position of {100} Bragg reflections was equal to 23.5 Å (Figure 8B). The intrahelix π -stacking distance calculated from the position of {001} reflection in the GIWAXS pattern was equal to 3.43 Å, which compares well with the distance of 3.26 \pm 0.03 Å extracted from the DFT geometry shown in Figure 7.

Most importantly, intermolecular hexagonal packing and intramolecular π -stacking was also clear in powder diffraction patterns obtained with as-purified, precipitated polymer powders (Figure 8C), with the values of helix diameter and π -stacking distance equal to respectively 22.7 and 3.37 Å. It should be noted that π -stacking distances observed here for the furan backbone are almost 0.5 Å shorter than those commonly reported for P3HT (\sim 3.8 Å), ⁴⁴ reflecting the impact of the size of the ring heteroatom (covalent radius of O = 1.32 Å and S = 2.1 Å).

The helical structure of P3HEF is also consistent with the nanoscale morphology of ultrathin films, which was investigated using tapping mode AFM. Polymer solutions (5 μ M) in

THF were cast onto freshly cleaved highly oriented pyrolytic graphite (HOPG). Phase contrast atomic force microscopy (AFM) images of such prepared samples (Figure 8D) revealed the presence of straight filamentous aggregates of uniform nanoparticulate objects, suggestive of cofacial stacking of individual helical assemblies. Analysis of the histogram of heights in the corresponding height images (Figure 8D, top inset) showed broad distribution of nano-object heights, centered around 2.2 nm, in good agreement with dynamic light scattering (DLS, bottom inset).

This value compares well with the effective outer diameter of P3HEF helices (25 \pm 1 Å) obtained by calculating the outer radius $R_{\rm out}$ from the equation in which P3HEF helices were treated as hollow cylindrical nanoobjects with a shell of density ρ composed of side chains with molar mass $M_{\rm side}$.

$$\pi (R_{\text{out}}^2 - R_{\text{in}}^2) = (M_{\text{side}} \tau) / (\psi N_{\text{A}} \rho)$$
 (1)

The shells were assumed to contain τ side chains per helix turn at pitch ψ surrounding the cylindrical conjugated core of radius $R_{\rm in}$ ($N_{\rm A}$ is the Avogadro's constant). The values of τ , ψ , and $R_{\rm in}$ used in this estimate were extracted from the geometry of the tridecamer of 3-methyl ester furan modeled by DFT (Figure 7).

UV–Vis Absorption Spectroscopy. The UV–vis spectrum for P3HEF is a dramatic indicator of the difference between the ester-functionalized furan and its sister homopolymer P3HF (Figure 9). The observed $\lambda_{\rm max}$ of P3HEF at ~331 nm (with tailing into the visible region) is blue-shifted by ~130 nm relative to P3HF ($\lambda_{\rm max}$ = 460 nm) in solution. This unusual spectrum is a manifestation of optical selection rules resulting from the helical conformation of the polymer.

In a flat conjugated linear chain with all repeat units *anti* (such as in P3HF or P3HT), the lowest energy $\pi - \pi^*$ transition has a large oscillator strength arising from the linear alignment of the transition dipoles of the polymer units along

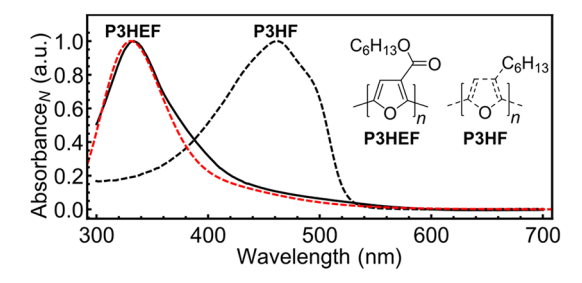


Figure 9. Normalized absorption spectra of P3HEF (left) and its alkyl side chain analogue (P3HF) collected in THF. The red trace corresponds to the predicted UV—vis spectrum from TD-DFT of the *syn* methylfuran 3-carboxylate 13-mer (CAM-B3LYP 6-31G(d,p)).

the chain axis. In contrast, in a macrocycle the lowest energy $\pi-\pi^*$ transition is forbidden (zero oscillator strength) due to the cancellation of the transition dipole vectors when summed along the circumference of the circle. The optical intensity instead goes to a higher energy $\pi-\pi^*$ transition, as has been demonstrated previously with macrocyclic oligothiophenes (all-syn repeat units). For a helical polymer, the absorption spectra show signatures of both of these behaviors. For light polarized along the helix axis, the transition dipoles of the units are aligned and the HOMO–LUMO transition carries the bulk of the intensity. For light polarized perpendicular to the helix axis, the optical intensity is instead shifted to a higher lying $\pi-\pi^*$ transition.

To illustrate how these trends evolve in all-syn and all-anti P3HEF oligomers of different lengths, UV-vis spectra were computed using time-dependent (TD)-DFT (Figure 10). The anti conformers produced the expected red-shift of the lowest energy transition, which arises predominantly from the $\pi-\pi^*$ HOMO-LUMO excitation (I in Figure 10A). This transition has the largest oscillator strength and is clearly the largest contributor to the computed spectrum. By contrast, the simulated UV-vis spectra evolve quite differently in the helical conformer (Figure 10B).

For the dimer to the pentamer, the oligomers are perfectly flat with a 0° dihedral angle between repeat units (see relevant xyz files included in the Supporting Information and Figure S49 for the pentamer). In the hexamer, steric strain between the oligomer ends produces a small dihedral angle between the rings (between 6° and 10°), which can be considered as the first turn to form the helix. As the length of the syn oligomer is increased, the circular arrangement of transition dipole vectors leads to cancellations that lower the intensity of the lowest energy $\pi-\pi^*$ HOMO-LUMO excitation (I in Figure 10B). Beyond the hexamer, the helix has undergone a full turn and the optical intensity has been transferred to higher energy $\pi-\pi^*$ transitions (III), corresponding to transitions between the HOMO and higher energy unoccupied orbitals such as the LUMO+3 and LUMO+4.

Note that this blue-shift is a result of optical selection rules and does not reflect a loss of conjugation in the helical geometry. In fact, the computed red-shift in the HOMO—

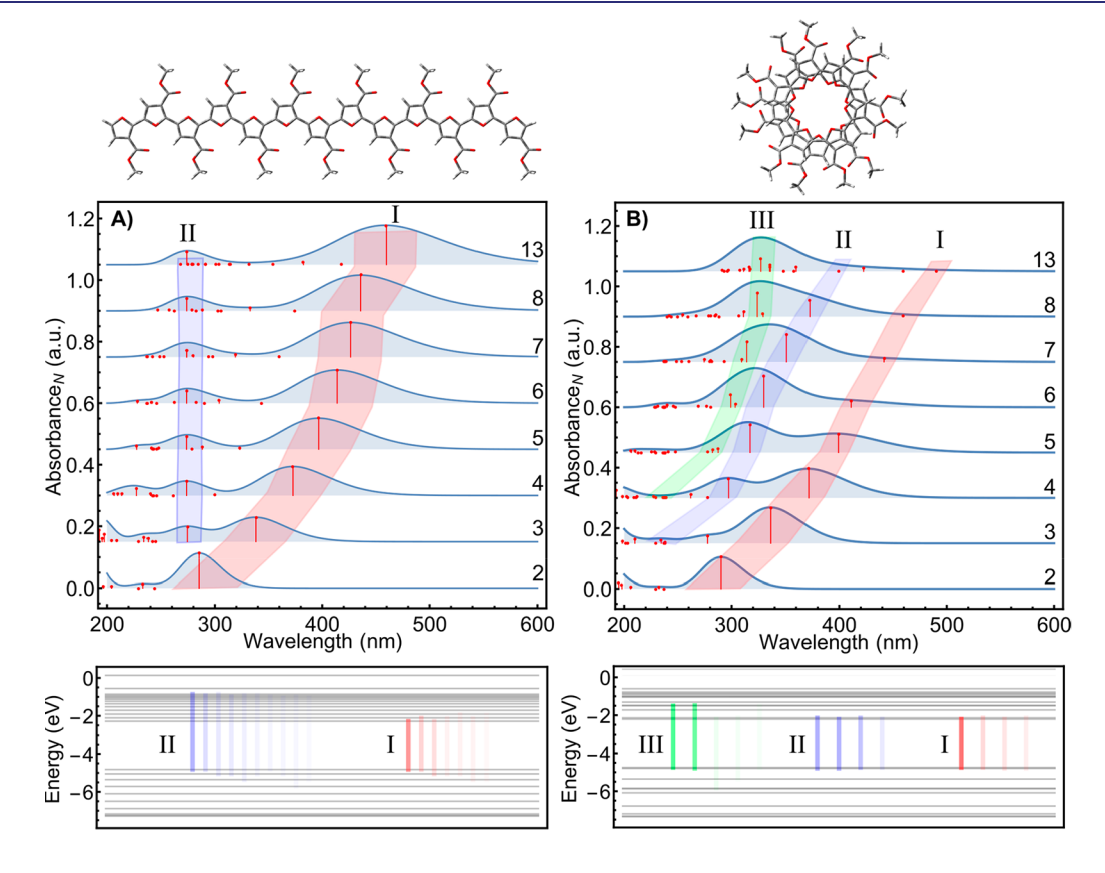


Figure 10. UV—vis spectra for a series of oligomers constructed from methyl furan-3-carboxylate predicted by TD-DFT calculations (CAM-B3LYP 6-31G(d,p)). (A) (Top) UV—vis spectra for oligomers with an *anti* arrangement of the repeat units. (Bottom) Orbital contributions to the predicted transitions with color intensity for the line corresponding to degree of contribution. (B) (Top) UV—vis spectra for oligomers with a *syn* arrangement of the repeat units. (Bottom) Orbital contributions to the predicted transitions with color intensity for the line corresponding to degree of contribution.

LUMO transition is nearly identical to that in the linear *anti* configuration, indicating that the helix retains high conjugation. The computed spectra of the linear oligomers also show an additional, weak transition near 280 nm (II in Figure 10A). For *syn* oligomers with 8 or fewer units, the spectra suggest that some mixing occurs between the electronic states responsible for the II and III spectral features.

The TD-DFT spectrum of the helical ester-substituted tridecamer matches almost perfectly with the experimental spectrum from the polymer (dashed red trace in Figure 9). On this basis, we assign the absorption edge to the HOMO-LUMO transition and the two transitions with largest oscillator strength (near 330 nm) to transitions between the HOMO and higher energy unoccupied orbitals such as the LUMO+3 and LUMO+4 (labeled III in Figure 10B). The TD-DFT calculations shown in Figure 10 are critical for elucidating the origin of an unusual shape of the UV-vis spectra of helical species. In particular, they explain why the optical band gap of the helical polymer needs to be determined from the lowenergy tail of the spectrum, which corresponds to the weakly allowed HOMO-LUMO transition rather than by extrapolation from the prominent higher energy transition. A rough estimation carried out based on where the UV-vis spectrum of P3HEF in solution or in the solid-state nears zero absorbance (Figure S54) yielded a value of 2.1 eV. This value is quite close to that determined for P3HF (\sim 2.2 eV) 46 and is similar to the optical band gaps determined for several helical polythiophenes synthesized recently ($E_{\rm g} \approx 2.3 - 2.5 \; {\rm eV}$). ^{47,48} Cyclic Voltammetry. CV was used to determine the

Cyclic Voltammetry. CV was used to determine the electrochemical band gap and compare the electrochemical behavior of P3HEF to previously reported polyfurans that were measured under similar conditions. The CV experiment was conducted by drop-casting P3HEF onto a glassy-carbon electrode, and potentials were referenced to the saturated calomel electrode (SCE) (using the ferrocene/ferrocenium redox couple). Previous reports indicate that unsubstituted polyfuran (PF) and poly(3-octylfuran) oxidize between 0.7 and 0.75 V (vs SCE) when using NBu₄PF₆ as the supporting electrolyte. For P3HEF, we obtained a value of $E_{\rm pa}\approx 0.95$ V, which displayed quasi-reversible behavior (Figure 11). The

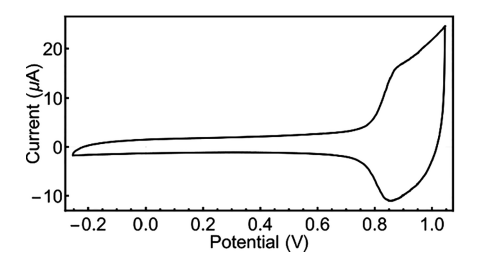


Figure 11. Cyclic voltammogram of P3HEF to illustrate quasi-reversible oxidation of the polymer. P3HEF was drop cast on a glassy carbon electrode and the trace was recorded at a scan rate of 100 mV/s in degassed MeCN with NBu₄PF₆ as the supporting electrolyte (0.1 M). The voltammogram was referenced using Fc/Fc⁺ as an internal standard (0.4 V vs SCE).

P3HEF polymer film could be cycled from -1.0 V to +1.3 V without any marked changes in the oxidation behavior. It should be noted, however, that sweeping to more negative reduction potentials produced a large irreversible reduction at $E_{\rm pc} = -1.86$ V, with a much larger peak current than for the oxidation wave (Figure S31). The appearance of this signal is

indicative of an irreversible change of the polymer, as no oxidation signal that could be attributed to the polymer is present upon return to positive potentials. In fact, several new unassigned signals appear in the electrochemical window upon cycling after reduction (Figure S31), most likely pointing to the polymer degradation upon reduction. The determination of the electrochemical band gap of P3HEF from the onsets of oxidation and reduction (+0.79 and -1.75 V, respectively) yielded the value of E_{σ} = 2.54 eV, which is comparable with the optical band gap determined from the UV-vis spectrum as discussed earlier. It is also similar to the values reported previously for nonhelical polyfurans (~2.2-2.7 eV). 1,2,46,49 Most importantly, all these results indicate that the adoption of a helical conformation by P3HEF chains does not lead to any appreciable loss of conjugation, which would limit the potential value of these materials as building blocks for organic electronics.

Bond Alternation Patterns. Further insights into the extent of conjugation along the backbone were obtained by comparing the bond alternation patterns in DFT-optimized geometries of the P3HEF tridecamer in all-*syn* and all-*anti* configurations (Figure 12). The bond alternation patterns for carbon—carbon bonds along the backbone were virtually indistinguishable, further confirming the preservation of conjugation in the helix.

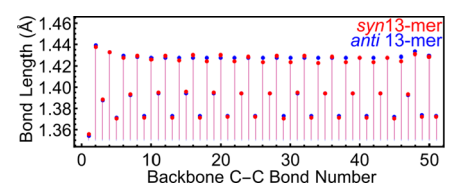


Figure 12. C=C and C-C bond lengths plotted as a function of the bond alternation pathway along the oligomer backbone for the *syn* and *anti* ester-substituted structures. The atom numbering starts from the carbon distal from the ester group.

Circular Dichroism. As expected, the solution CD spectra of P3HEF did not reveal any appreciable dichroism (racemic mixture of left- and right-handed helices). To explore the possibility of imparting helical chirality, we have synthesized a variant of the polymer in which the achiral hexyl ester side chains were replaced with branched chiral 1-ethylhexyl counterparts (see Supporting Information for synthetic details).

The UV-vis spectrum of (S)-P3EHEF acquired in CHCl₃ differed starkly from that observed for P3HEF and was composed of two major bands at 330 and 445 nm (Figure 13, top, red trace). Likewise, the CD spectrum acquired in the same solvent confirmed the chiral nature of the polymer (Figure 13, bottom, red trace). Most interestingly, both the absorption and CD spectra changed markedly upon gradual introduction of a nonsolvent (CH₃OH). The band at 445 nm diminished, until the spectrum closely resembled the one observed for P3HEF upon reaching a CHCl₃:CH₃OH ratio of 40:60. Concomitantly, the introduction of CH₃OH led to marked enhancement of the CD signal (Figure 13, bottom). This evolution of the UV-vis absorption and CD spectra upon the introduction of a nonsolvent can be interpreted as evidence of transition of a polymer conformation from a partially unfolded (disordered) state in a good solvent to a compact, helical state observed for P3HEF. It is likely that such partial

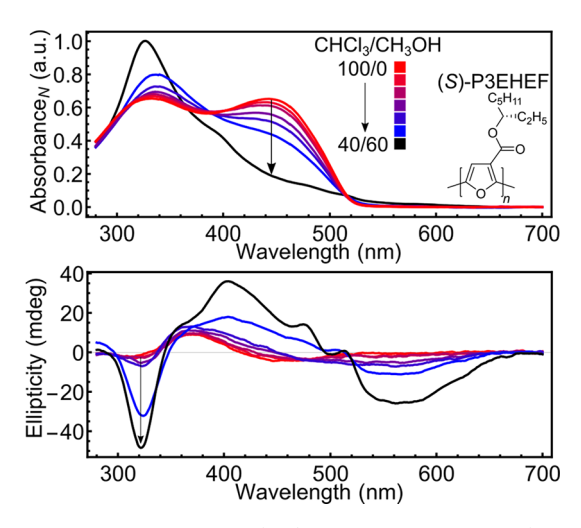


Figure 13. UV-vis absorption (top) and circular dichroism (bottom) spectra of 0.02 mg/mL solutions of 11.7 kDa (S)-P3EHEF illustrating the conformational change upon addition of a nonsolvent (CH₃OH).

unfolding in a good solvent results from destabilization of the helical structure caused by the steric interactions from the fully solvated bulky, branched chiral side-chain substituents. Upon addition of a nonsolvent, the compact helical assembly is completely re-formed.

Interestingly, the chiral variant (S)-P3EHEF is highly fluorescent in CHCl₃. The fluorescence is lost upon titration with CH₃OH (Figure 14), again indicating formation of the compact helical assembly for which the radiative transition from the lowest excited state is strongly disallowed, as discussed earlier.

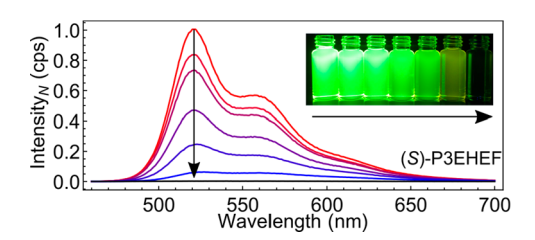


Figure 14. Fluorescence spectra of 0.02 mg/mL solutions of 11.7 kDa (S)-P3EHEF in CHCl₃ (top bright red trace) illustrating the loss of fluorescence with increasing CH₃OH content ranging from 10% to 60% volume. Excitation wavelength: 440 nm.

The unfolding/folding transition of (S)-P3EHEF was also manifested by the evolution of the ¹H NMR spectra taken under different solvation conditions. In a good solvent (CDCl₃) the line shapes were sharp and well-defined, with characteristic narrow signals originating from the aromatic and methine carbon protons appearing respectively at 7.78 and 5.05 ppm (Figure S32). As expected for the formation of folded helical structures, all lines in the ¹H NMR spectra broadened upon introduction of the nonsolvent (Figure S39). Altogether, these four different spectroscopic techniques provide evidence for reversible changes in helix behavior and provide a means to monitor formation of the compact helical assembly.

To confirm that both left- and right-handed helices are accessible, the polymer (R)-P3EHEF with the opposite handedness was synthesized. As expected, the CD spectrum of such a synthesized polymer taken in a CHCl₃:CH₃OH

mixture was inverted in comparison with its previous counterpart (Figure 15).

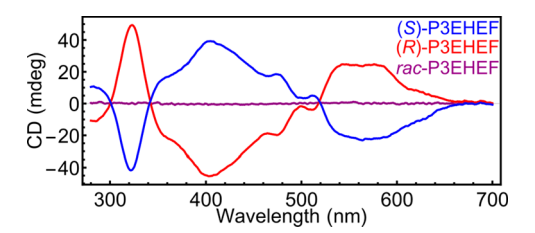


Figure 15. Circular dichroism spectra of (S)-P3EHEF (11.7 kDa), (R)-P3EHEF (10.2 kDa), and rac-P3EHEF (10.2 kDa) acquired in a 40:60 CHCl₃-CH₃OH mixture (0.02 mg/mL solutions). The two chiral variants exhibited the expected mirror image relationships.

CONCLUSIONS

In conclusion, a new class of ester-functionalized polyfurans was synthesized and shown to be significantly more photostable than their alkyl analogue. The steric factors imparted by ester substituents (lone pair repulsion between ring oxygen atoms in the main chain and the carbonyl oxygens in side-chain ester groups) force the adjacent rings to adopt an all-syn configuration, leading to the formation of compact, π -stacked helical structures. The helical structures are further stabilized by the intramolecular hydrogen bonding between carbonyl oxygens and hydrogens on the rings. Given their compact helical structure, these newly synthesized polyfurans can be classified as conjugated organic nanoparticles, with a highly ordered hollow π -stacked conjugated core surrounded by the soft insulating outer layer.

Importantly, presented results demonstrate that this new class of foldamer macromolecules can be synthesized using catalyst-transfer polycondensation. Despite being formally classified as polycondenstation, and thus expected to proceed via a step-growth mechanism, CTP is known to proceed in chain-growth fashion. This opens the way to the precise control of polymer chain lengths (and thus nanoparticle sizes) with degrees of polymerization as high as 100 repeat units. Furthermore, the nearly living character of CTP makes it possible to produce chains with complex architecture⁵ and sequence, 50,51 pointing to the possibility of further exploring the analogies between synthetic foldamers and biological macromolecules. The conjugated nature of the polyfuran backbones is expected to give rise to useful electronic, optical, and magneto-optical properties, which will be the subject of future studies.

Many potential future avenues exist for exploring these materials. Given their high stability in solution, these helical furan nanoparticles could be subjected to further chemical transformations, since the ester side chains provide a perfect location for postpolymerization modification. Control of folding patterns/stability may be tunable by varying the sequence of repeat units along the backbone. The use of living polymerization opens the way to the integration within block copolymers, enabling assembly of larger scale structures and architectures. The presence of a 0.4 nm diameter inner cavity lined with oxygen atoms may allow for hosting a range of small guest molecules and ions. In a broader perspective, the foldamer introduced here has the potential to be used as a supramolecular platform with a wide range of potential applications in electro/photocatalytic chemistry.

ASSOCIATED CONTENT

Supporting Information

The Supporting Information is available free of charge on the ACS Publications website at DOI: 10.1021/jacs.9b01567.

Experimental procedures, NMR spectra, DFT parameters, computed structures (PDF)

X-ray crystallography information (CIF)

Optimized geometries for the computed structures (ZIP)

Optimized geometries for the computed structures (ZIP)

AUTHOR INFORMATION

Corresponding Authors

*noonan@andrew.cmu.edu

*tomek@andrew.cmu.edu

ORCID ®

Yunyan Qiu: 0000-0001-9279-4714 David Yaron: 0000-0001-8485-8685 Stefan Bernhard: 0000-0002-8033-1453 Kevin J. T. Noonan: 0000-0003-4061-7593 Tomasz Kowalewski: 0000-0002-3544-554X

Notes

The authors declare no competing financial interest.

ACKNOWLEDGMENTS

K.J.T.N. is grateful to the ARO (W911NF-16-1-0053) and NSF for a Career Award (CHE-1455136). S.B. is also grateful to NSF for support (CHE-1764353). K.J.T.N. thanks Geoff Hutchison (University of Pittsburgh), Sam Gellman (University of Wisconsin), Catalina Achim (CMU), and Bruce Armitage (CMU) for helpful discussions. Finally, the authors are also grateful to Linda Peteanu (CMU) and Stephanie Kramer for their help with fluorescence measurements.

REFERENCES

- (1) Glenis, S.; Benz, M.; LeGoff, E.; Schindler, J. L.; Kannewurf, C. R.; Kanatzidis, M. G. Polyfuran: a new synthetic approach and electronic properties. *J. Am. Chem. Soc.* **1993**, *115*, 12519–12525.
- (2) Politis, J. K.; Nemes, J. C.; Curtis, M. D. Synthesis and Characterization of Regiorandom and Regioregular Poly(3-octylfuran). J. Am. Chem. Soc. 2001, 123, 2537–2547.
- (3) Baker, M. A.; Tsai, C.-H.; Noonan, K. J. T. Diversifying Cross-Coupling Strategies, Catalysts and Monomers for the Controlled Synthesis of Conjugated Polymers. *Chem. Eur. J.* **2018**, *24*, 13078–13088.
- (4) Verheyen, L.; Leysen, P.; Van den Eede, M.-P.; Ceunen, W.; Hardeman, T.; Koeckelberghs, G. Advances in the Controlled Polymerization of Conjugated Polymers. *Polymer* **2017**, *108*, 521–546.
- (5) Yokozawa, T.; Ohta, Y. Transformation of Step-Growth Polymerization into Living Chain-Growth Polymerization. *Chem. Rev.* **2016**, *116*, 1950–1968.
- (6) Bryan, Z. J.; McNeil, A. J. Conjugated Polymer Synthesis via Catalyst-Transfer Polycondensation (CTP): Mechanism, Scope, and Applications. *Macromolecules* **2013**, *46*, 8395–8405.
- (7) Kiriy, A.; Senkovskyy, V.; Sommer, M. Kumada Catalyst-Transfer Polycondensation: Mechanism, Opportunities, and Challenges. *Macromol. Rapid Commun.* **2011**, *32*, 1503–1517.
- (8) Okamoto, K.; Luscombe, C. K. Controlled Polymerizations for the Synthesis of Semiconducting Conjugated Polymers. *Polym. Chem.* **2011**, *2*, 2424–2434.

- (9) Yokozawa, T.; Yokoyama, A. Chain-Growth Condensation Polymerization for the Synthesis of Well-Defined Condensation Polymers and π -Conjugated Polymers. *Chem. Rev.* **2009**, *109*, 5595–5619
- (10) Yashima, E.; Ousaka, N.; Taura, D.; Shimomura, K.; Ikai, T.; Maeda, K. Supramolecular Helical Systems: Helical Assemblies of Small Molecules, Foldamers, and Polymers with Chiral Amplification and Their Functions. *Chem. Rev.* **2016**, *116*, 13752–13990.
- (11) Yashima, E. Synthesis and structure determination of helical polymers. *Polym. J.* **2010**, 42, 3–16.
- (12) Yashima, E.; Maeda, K.; Iida, H.; Furusho, Y.; Nagai, K. Helical Polymers: Synthesis, Structures, and Functions. *Chem. Rev.* **2009**, *109*, 6102–6211.
- (13) Foldamers: Structure, Properties, and Applications; Hecht, S.; Huc, I., Eds.; Wiley-VCH: Weinheim, 2007.
- (14) Nakano, T.; Okamoto, Y. Synthetic Helical Polymers: Conformation and Function. Chem. Rev. 2001, 101, 4013-4038.
- (15) Kushida, S.; Oki, O.; Saito, H.; Kuwabara, J.; Kanbara, T.; Tashiro, M.; Katouda, M.; Imamura, Y.; Yamamoto, Y. From Linear to Foldamer and Assembly: Hierarchical Transformation of a Coplanar Conjugated Polymer into a Microsphere. *J. Phys. Chem. Lett.* 2017, 8, 4580–4586.
- (16) Handbook of Thiophene-Based Materials: Applications in Organic Electronics and Photonics; Perepichka, I. F.; Perepichka, D. F., Eds.; John Wiley & Sons, Ltd: Chichester, UK, 2009.
- (17) Sheberla, D.; Patra, S.; Wijsboom, Y. H.; Sharma, S.; Sheynin, Y.; Haj-Yahia, A.-E.; Barak, A. H.; Gidron, O.; Bendikov, M. Conducting polyfurans by electropolymerization of oligofurans. *Chem. Sci.* **2015**, *6*, 360–371.
- (18) Gidron, O.; Bendikov, M. α -Oligofurans: An Emerging Class of Conjugated Oligomers for Organic Electronics. *Angew. Chem., Int. Ed.* **2014**, 53, 2546–2555.
- (19) Jin, X.-H.; Sheberla, D.; Shimon, L. J. W.; Bendikov, M. Highly Coplanar Very Long Oligo(alkylfuran)s: A Conjugated System with Specific Head-To-Head Defect. *J. Am. Chem. Soc.* **2014**, *136*, 2592–2601.
- (20) Gidron, O.; Dadvand, A.; Wei-Hsin Sun, E.; Chung, I.; Shimon, L. J. W.; Bendikov, M.; Perepichka, D. F. Oligofuran-containing molecules for organic electronics. *J. Mater. Chem. C* **2013**, *1*, 4358–4367.
- (21) Gidron, O.; Diskin-Posner, Y.; Bendikov, M. High Charge Delocalization and Conjugation in Oligofuran Molecular Wires. *Chem. Eur. J.* **2013**, *19*, 13140–13150.
- (22) Gidron, O.; Dadvand, A.; Sheynin, Y.; Bendikov, M.; Perepichka, D. F. Towards "green" electronic materials. α -Oligofurans as semiconductors. *Chem. Commun.* **2011**, *47*, 1976–1978.
- (23) Gidron, O.; Diskin-Posner, Y.; Bendikov, M. α -Oligofurans. *J. Am. Chem. Soc.* **2010**, 132, 2148–2150.
- (24) Sharma, S.; Zamoshchik, N.; Bendikov, M. Polyfurans: A Computational Study. *Isr. J. Chem.* **2014**, *54*, 712–722.
- (25) Sharma, S.; Bendikov, M. α -Oligofurans: A Computational Study. *Chem. Eur. J.* **2013**, *19*, 13127–13139.
- (26) Yiu, A. T.; Beaujuge, P. M.; Lee, O. P.; Woo, C. H.; Toney, M. F.; Fréchet, J. M. J. Side-Chain Tunability of Furan-Containing Low-Band-Gap Polymers Provides Control of Structural Order in Efficient Solar Cells. J. Am. Chem. Soc. 2012, 134, 2180–2185.
- (27) Woo, C. H.; Beaujuge, P. M.; Holcombe, T. W.; Lee, O. P.; Fréchet, J. M. J. Incorporation of Furan into Low Band-Gap Polymers for Efficient Solar Cells. *J. Am. Chem. Soc.* **2010**, *132*, 15547–15549.
- (28) Montagnon, T.; Kalaitzakis, D.; Triantafyllakis, M.; Stratakis, M.; Vassilikogiannakis, G. Furans and Singlet Oxygen Why There is More to Come From This Powerful Partnership. *Chem. Commun.* **2014**, *50*, 15480–15498.
- (29) Zamadar, M.; Greer, A. Singlet Oxygen as a Reagent in Organic Synthesis. In *Handbook of Synthetic Photochemistry*; Albini, A.; Fagnoni, M., Eds.; Wiley-VCH: Weinheim, Germany, 2009.
- (30) Kappe, C. O.; Murphree, S. S.; Padwa, A. Synthetic Applications of Furan Diels-Alder Chemistry. *Tetrahedron* **1997**, *53*, 14179–14233.

- (31) Qiu, Y.; Worch, J. C.; Fortney, A.; Gayathri, C.; Gil, R. R.; Noonan, K. J. T. Nickel-Catalyzed Suzuki Polycondensation for Controlled Synthesis of Ester-Functionalized Conjugated Polymers. *Macromolecules* **2016**, *49*, 4757–4762.
- (32) Fuji, K.; Tamba, S.; Shono, K.; Sugie, A.; Mori, A. Murahashi Coupling Polymerization: Nickel(II)-N-Heterocyclic Carbene Complex-Catalyzed Polycondensation of Organolithium Species of (Hetero)arenes. *J. Am. Chem. Soc.* **2013**, *135*, 12208–12211.
- (33) Tamba, S.; Shono, K.; Sugie, A.; Mori, A. C—H Functionalization Polycondensation of Chlorothiophenes in the Presence of Nickel Catalyst with Stoichiometric or Catalytically Generated Magnesium Amide. J. Am. Chem. Soc. 2011, 133, 9700–9703.
- (34) Wong, M.; Hollinger, J.; Kozycz, L. M.; McCormick, T. M.; Lu, Y.; Burns, D. C.; Seferos, D. S. An Apparent Size-Exclusion Quantification Limit Reveals a Molecular Weight Limit in the Synthesis of Externally Initiated Polythiophenes. *ACS Macro Lett.* **2012**, *1*, 1266–1269.
- (35) Winter, J. D.; Deshayes, G.; Boon, F.; Coulembier, O.; Dubois, P.; Gerbaux, P. MALDI-ToF analysis of polythiophene: use of trans-2-[3-(4-t-butyl-phenyl)-2-methyl-2-propenylidene]malononitrile—DCTB—as matrix. J. Mass Spectrom. 2011, 46, 237–246.
- (36) Bloom, J. W. G.; Wheeler, S. E. Benchmark Torsional Potentials of Building Blocks for Conjugated Materials: Bifuran, Bithiophene, and Biselenophene. *J. Chem. Theory Comput.* **2014**, *10*, 3647–3655.
- (37) Fabiano, E.; Della Sala, F. Torsional potential of π-conjugated molecules using the localized Hartree–Fock Kohn–Sham exchange potential. *Chem. Phys. Lett.* **2006**, *418*, 496–501.
- (38) van Eijck, L.; Johnson, M. R.; Kearley, G. J. Intermolecular Interactions in Bithiophene as a Model for Polythiophene. *J. Phys. Chem. A* **2003**, *107*, 8980–8984.
- (39) Steiner, T.; Kanters, J. A.; Kroon, J. Acceptor Directionality of Sterically Unhindered C-H···O = C Hydrogen Bonds Donated by Acidic C-H Groups. *Chem. Commun.* **1996**, 1277–1278.
- (40) Steiner, T. Unrolling the Hydrogen Bond Properties of C-H··· O Interactions. *Chem. Commun.* **1997**, 727–734.
- (41) Dubus, S.; Marceau, V.; Leclerc, M. Helical Conjugated Polymers by Design. *Macromolecules* **2002**, *35*, 9296–9299.
- (42) Hill, D. J.; Mio, M. J.; Prince, R. B.; Hughes, T. S.; Moore, J. S. A Field Guide to Foldamers. *Chem. Rev.* **2001**, *101*, 3893–4011.
- (43) Dufresne, G.; Bouchard, J.; Belletête, M.; Durocher, G.; Leclerc, M. Thermochromic and Solvatochromic Conjugated Polymers by Design. *Macromolecules* **2000**, *33*, 8252–8257.
- (44) Duong, D. T.; Wang, C.; Antono, E.; Toney, M. F.; Salleo, A. The chemical and structural origin of efficient p-type doping in P3HT. *Org. Electron.* **2013**, *14*, 1330–1336.
- (45) Bednarz, M.; Reineker, P.; Mena-Osteritz, E.; Bäuerle, P. Optical absorption spectra of linear and cyclic thiophenes—selection rules manifestation. *J. Lumin.* **2004**, *110*, 225–231.
- (46) Qiu, Y.; Fortney, A.; Tsai, C.-H.; Baker, M. A.; Gil, R. R.; Kowalewski, T.; Noonan, K. J. T. Synthesis of Polyfuran and Thiophene-Furan Alternating Copolymers Using Catalyst-Transfer Polycondensation. *ACS Macro Lett.* **2016**, *5*, 332–336.
- (47) Wang, P.; Jeon, I.; Lin, Z.; Peeks, M. D.; Savagatrup, S.; Kooi, S. E.; Van Voorhis, T.; Swager, T. M. Insights into Magneto-Optics of Helical Conjugated Polymers. *J. Am. Chem. Soc.* **2018**, *140*, 6501–6508
- (48) Leysen, P.; Teyssandier, J.; De Feyter, S.; Koeckelberghs, G. Controlled Synthesis of a Helical Conjugated Polythiophene. *Macromolecules* **2018**, *51*, 3504–3514.
- (49) Distefano, G.; Jones, D.; Guerra, M.; Favaretto, L.; Modelli, A.; Mengoli, G. Determination of the Electronic-Structure of Oligofurans and Extrapolation to Polyfuran. *J. Phys. Chem.* **1991**, *95*, 9746–9753.
- (50) Tsai, C.-H.; Fortney, A.; Qiu, Y. Y.; Gil, R. R.; Yaron, D.; Kowalewski, T.; Noonan, K. J. T. Conjugated Polymers with Repeated Sequences of Group 16 Heterocycles Synthesized through Catalyst-Transfer Polycondensation. *J. Am. Chem. Soc.* **2016**, *138*, 6798–6804.
- (51) Fortney, A.; Tsai, C.-H.; Banerjee, M.; Yaron, D.; Kowalewski, T.; Noonan, K. J. T. Impact of Precise Control over Microstructure in

Thiophene-Selenophene Copolymers. *Macromolecules* **2018**, *51*, 9494–9501.